Semiconductors

Titanium Trisulfide Monolayer: Theoretical Prediction of a New Direct-Gap Semiconductor with High and Anisotropic Carrier Mobility**

Jun Dai and Xiao Cheng Zeng*

Abstract: *A new two-dimensional (2D) layered material, namely, titanium trisulfide (TiS_3) monolayer, is predicted to possess novel electronic properties. Ab initio calculations show that the perfect TiS_3 monolayer is a direct-gap semiconductor with a bandgap of 1.02 eV, close to that of bulk silicon, and with high carrier mobility. More remarkably, the in-plane electron mobility of the 2D TiS_3 is highly anisotropic, amounting to about $10\,000\ cm^2\,V^{-1}\,s^{-1}$ in the b direction, which is higher than that of the MoS_2 monolayer, whereas the hole mobility is about two orders of magnitude lower. Furthermore, TiS_3 possesses lower cleavage energy than graphite, suggesting easy exfoliation for TiS_3. Both dynamical and thermal stability of the TiS_3 monolayer is examined by phonon-spectrum calculation and Born–Oppenheimer molecular dynamics simulation. The desired electronic properties render the TiS_3 monolayer a promising 2D atomic-layer material for applications in future nanoelectronics.*

The successful isolation of two-dimensional (2D) graphene in 2004[1] has greatly boosted research interests in 2D materials with intralayer covalent bonding and interlayer van der Waals (vdW) bonding.[2] Except for graphene,[3] the family of 2D crystals also includes transition-metal dichalcogenides (TMDCs),[2a,4] hexagonal boron nitride (h-BN),[5] silicene,[6] germanene,[7] and phosphorene.[8] These 2D crystals are not only geometrically interesting as they represent the thinnest form of crystalline solids that can be formed, but also exhibit many new exotic condensed matter phenomena that are absent in their bulk counterparts.[2a,4b] For example, a single graphene layer is a zero-gap semiconductor with a linear Dirac-like dispersion near the Fermi level whereas graphite is known to show a semimetallic behavior with a bandgap overlap of about 41 meV.[9] A MoS_2 monolayer sheet possesses a direct bandgap of ca. 1.8 eV, whereas its bulk phase has an indirect bandgap of 1.29 eV.[10] The bandgap of the recently isolated few layer phosphorene (2D form of black phosphorus) is also highly layer-dependent, ranging from ca. 1.5 eV for the monolayer to ca. 0.3 eV for the bulk.[8b,11]

2D-layered materials offer opportunities for a variety of applications, particularly in next-generation electronic devices such as field-effect transistors (FET) and logic circuits. For high-performance FET applications, a 2D material should possess a moderate bandgap and reasonably high in-plane carrier mobility. Graphene is a highly promising 2D material for high-speed nanotransistors due to its massless charge carriers. However, it lacks a bandgap for controllable operations.[12] The molybdenum disulfide (MoS_2) monolayer sheets are more promising for FET applications as not only they possess a direct bandgap of ca. 1.8 eV,[10] but also the 2D MoS_2-based FET devices show good performance with a high on/off ratio of about 10^8 as well as a carrier mobility of ca. $200\ cm^2\,V^{-1}\,s^{-1}$. The latter can be enhanced even up to $500\ cm^2\,V^{-1}\,s^{-1}$ with improvement.[13] Also, recent experiments demonstrated that FET devices built upon few-layer phosphorene exhibit reasonably high on/off ratio (up to 10^4) and appreciably high hole mobility of ca. $55\ cm^2\,V^{-1}\,s^{-1}$ (at a thickness of ≈ 5 nm) to ca. $1000\ cm^2\,V^{-1}\,s^{-1}$ (at a thickness of ≈ 10 nm).[8] Nevertheless, new 2D-layered materials with moderate direct bandgap and high carrier mobility are still highly sought. In this work, we show an ab initio calculation evidence of a new 2D-layered material—the TiS_3 monolayer sheet—with the desired electronic properties.

Historically, bulk materials such as graphite, TMDCs, and black phosphorus were studied well ahead of their 2D-layered-material counterparts. Likewise, properties of bulk TiS_3 are known much earlier than those of 2D form. Bulk TiS_3 has a monoclinic crystalline structure (with the space group of p21m), and the TiS_3 crystal can be viewed as stacked parallel sheets with each sheet being composed of 1D chains of triangular TiS_3 unit. These sheets interact with one another through vdW forces.[14] It is also known that materials with stacking-layer structures can be a good precursor for contriving 2D atomic layers either by exfoliation[15] or by mechanical cleavage.[16] Indeed, layered TiS_3 has been proposed as a possible candidate for exfoliation.[2b] However, little research has been done toward isolation of the 2D TiS_3 sheet due to the lack of knowledge on the properties of TiS_3 monolayer, such as its desirable direct bandgap. To date, several electrical and transport measurements of bulk TiS_3 have been reported,[17] showing that the bulk TiS_3 is an n-type semiconductor with carrier mobility of ca. $30\ cm^2\,V^{-1}\,s^{-1}$ at room temperature. The mobility can be further enhanced up to about $100\ cm^2\,V^{-1}\,s^{-1}$ at the low temperature 100 K.[17a] Moreover, optical absorption measurements indicate that the bulk TiS_3 exhibits an optical gap about 1 eV.[18] More importantly, several recent experiments demonstrate that macroscopic films of TiS_3 ribbons with a thickness of

[*] Dr. J. Dai, Prof. X. C. Zeng
Department of Chemistry, University of Nebraska-Lincoln
Lincoln, NE 68588 (USA)
E-mail: xzeng1@unl.edu

hundreds of nanometers possess a direct bandgap of ca. 1.1 eV,[19] and few-layer TiS_3 nanoribbons-based devices (with a thickness of 10–30 nm) respond to wavelengths across the visible spectrum and show an ultrahigh photoresponse up to 2910 A/W.[20] The moderate bandgap of bulk TiS_3 coupled with relatively high carrier mobility renders the bulk TiS_3 a highly promising precursor for isolating 2D TiS_3 sheets with desired properties for nanoelectronic applications.

The PBE-D2 optimized structure of bulk TiS_3 is shown in Figure 1a, and the associated lattice constants are $a = 4.982$ Å, $b = 3.392$ Å, and $c = 8.887$ Å, and lattice angle $\beta = 97.24°$, all in very good agreement with the experimental

(a)
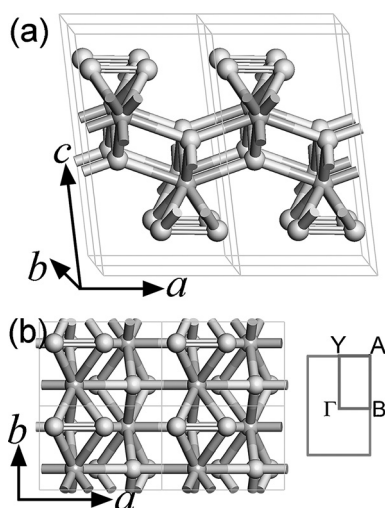
Figure 1. a) A $2\times2\times1$ supercell of the bulk TiS_3 structure, b) top view of a 2×2 TiS_3 monolayer sheet (left), and the first Brillouin zone and the high-symmetry points associated with the monolayer (right). The grey and white spheres refer to Ti and S atoms, respectively.

results, $a = 4.958$ Å, $b = 3.401$ Å, and $c = 8.778$ Å, and $\beta = 97.32°$.[14b] Furthermore, the computed band structures of the bulk TiS_3 from both PBE-D2 and HSE06 are shown in Figure S1 in the Supporting Information. PBE-D2 and HSE06 give qualitatively the same results except for the bandgap, because the PBE functional tends to underestimate the bandgap. Both PBE-D2 and HSE06 calculations indicate that the bulk TiS_3 is an indirect gap semiconductor from Γ (0, 0, 0) to Z (0, 0, 0.5). The PBE-D2 computation gives a bandgap of 0.21 eV, whereas HSE06 gives 1.02 eV. The latter agrees well with the measured optical gap which is around 1 eV.[18] The good agreement between the benchmark calculations and experiments for the bulk TiS_3 show that the theoretical methods chosen for this system is reliable. In addition, the band structures near the conduction band minimum (CBM) or the valence band maximum (VBM) of the bulk TiS_3 exhibit notable in-plane dispersion behavior (from Γ to Y (0, 0.5, 0)) or Γ to B (0.5, 0, 0)), indicating that the 2D TiS_3 monolayer sheet may have relatively high carrier mobility.

The computed HSE06 band structure and density of states (DOS) of the TiS_3 monolayer are shown in Figure 2a. Since the original Z point of the bulk TiS_3 folds back to the Γ point for the TiS_3 monolayer, the TiS_3 undergoes an indirect–direct

(b)
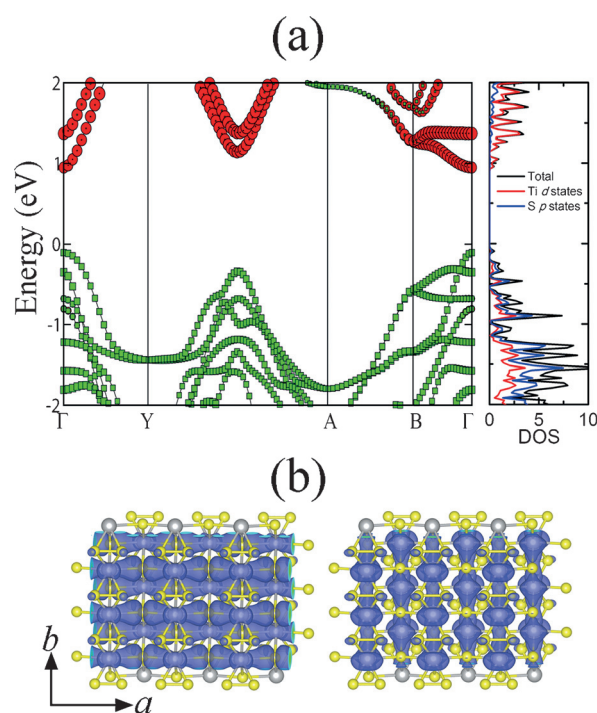
Figure 2. a) Computed HSE06 band structure of TiS_3 monolayer sheet; Γ (0.0, 0.0, 0.0), Y (0.0, 0.5, 0.0), A (0.5, −0.5, 0.0), B (0.5, 0.0, 0.0) refer to the special points in the first Brillouin zone; circles and rectangles refer to the contributions of Ti d states and S p states; and the Fermi level is set to zero; b) iso-surface plots of the charge density of VBM (left) and CBM (right) of the TiS_3 monolayer sheet, with an iso-value of 0.003 e/Bohr³.

transformation from an indirect bandgap semiconductor for the bulk to a direct bandgap semiconductor for the 2D monolayer counterpart, akin to the case of MoS_2.[10] Both VBM and CBM are located at the Γ point, yielding a direct bandgap of 1.06 eV. Moreover, from the orbital- and atom-projected DOS, we can see that the valance bands exhibit strong hybridization between the S p states and Ti d states from −2 eV to the top of valence band, whereas the conduction bands are mainly contributed by the d states of Ti (Figure 2a). The isosurface plots of the VBM and CBM are shown in Figure 2b, which show that the holes (from VBM) favor the a direction, whereas the electrons (from CBM) favor the b direction.

To compute the 2D elastic modulus (C) and the deformation-potential constant (E_1), we dilate the lattice of the cell up to 1.5% along both a and b directions, and then calculate the total energy and the positions of CBM and VBM with respect to the dilation. The atomic positions are relaxed at the dilation, and the electronic energies are calculated at the PBE-D2 level with ultrafine k-meshes ($35 \times 50 \times 1$). We note that although the PBE functional underestimates the bandgap, it can give quite good carrier mobility data for MoS_2,[21] graphyne,[22] graphene,[23] and graphdiyne.[24] The total energy–strain relation and the positions of CBM and VBM with respect to the strain are plotted in Figure 3. As shown in Figure 3b, the response of CBM and VBM to the applied strain appears to be highly anisotropic. The CBM
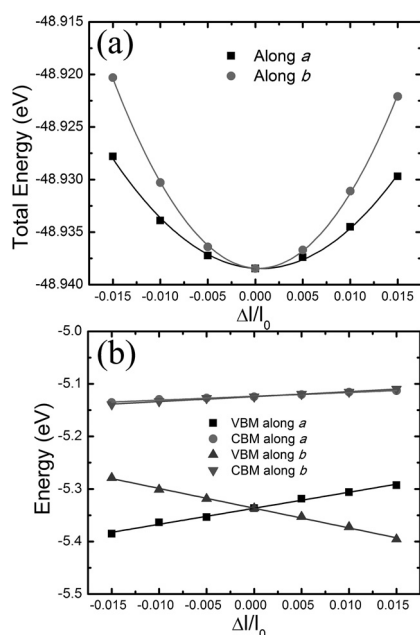
Figure 3. a) Strain–total energy relations and b) shifts of VBM and CBM under uniaxial strain along the *a* and *b* directions for TiS$_3$ monolayer sheet, Δl refers to the dilation along *a* or *b*, whereas l_0 refers to the lattice constant of *a* or *b* at equilibrium geometry. In (b), the vacuum level is set at zero for reference.

increases monotonously with the strain either along *a* or *b* direction, whereas the VBM decreases monotonously with the strain along the *b* direction but increases along *a*, resulting in bandgap increase due to the strain along *b* but bandgap decrease along *a*. The 2D modulus (*C*) is attained by the quadratic fitting of the total energy versus strain, and the deformation potential constant (E_1) is calculated by the linear fitting of the CBM (VBM)–strain relation. With *C*, E_1, and the effective mass known, the carrier mobilities are calculated by Equation (1). These data and the relaxation time ($\tau = \mu m^*/e$) are summarized in Table 1.

Table 1: Calculated deformation-potential constant (E_1), 2D modulus (*C*), effective mass (m^*), relaxation time (τ), and electron and hole mobility (μ) in *a* and *b* directions of the TiS$_3$ monolayer sheet at 300 K.

carrier type	E_1 [eV]	C [N/m]	m^* [m_e]	τ [ps]	μ [$\times 10^3$ cm^{2}V^{-1}s^{-1}]
electron (*a*)	0.73	81.29	1.47	0.84	1.01
hole (*a*)	3.05	81.29	0.32	0.22	1.21
electron (*b*)	0.94	145.05	0.41	3.23	13.87
hole (*b*)	−3.76	145.05	0.98	0.085	0.15

As shown in Table 1, the 2D modulus along *b* is nearly two times higher than that along the *a* direction. This is because the Ti–S bond strength along *a* is weaker than that along the *b* direction as the Ti–S bond length is 2.65 Å along *a* and 2.45 Å along *b*. The difference between the Ti–S bond strength along *a* and *b* also makes the deformation-potential constant along *b* larger than that along *a*, as the band energies are more sensitive to dilations along *b* than along *a*. The effective mass also shows an anisotropic feature: in *a* direction, the effective

mass of hole is much smaller than that of electron, whereas in the *b* direction, the effective mass of electron is about half of that of the hole. These results can be well explained by a charge–density plot of CBM and VBM as shown in Figure 2b in which one can see that VBM electrons are quite localized along *b*, whereas the CBM ones are delocalized along *b* but localized along *a*.

The predicted carrier mobilities of the perfect TiS$_3$ monolayer are highly anisotropic. The computed electron mobility along the *b* direction is 13.87×10^3 cm^{2}V^{-1}s^{-1}, about 14 times higher than that along the *a* direction (1.01×10^3 cm^{2}V^{-1}s^{-1}), whereas the hole mobility along the *a* direction is 1.21×10^3 cm^{2}V^{-1}s^{-1}, about eight times higher than that along the *b* direction (0.15×10^3 cm^{2}V^{-1}s^{-1}). It is worth to mention that the predicted carrier mobilities are notably higher than those of the MoS$_2$ monolayer sheet (which are in the range of 60–200 cm^{2}V^{-1}s^{-1}).[21] Especially, along the *b* direction, the electron mobility is about 100 times higher than the hole mobility, making the *b* direction more favorable for the electron conduction. The large difference in electron/hole mobility can be exploited for electron/hole separation.

Although the TiS$_3$ monolayer exhibits some novel properties for potential nanoelectronic applications, feasibility of isolation of the TiS$_3$ monolayer sheet by either exfoliation or mechanical cleavage techniques has yet to be confirmed. To examine this feasibility, we calculated the cleavage energy by introducing a fracture in the bulk TiS$_3$ (Figure 4b). To this end, the total energies under variation of the separation *d* between the fractured parts are computed to simulate the exfoliation process.[25] The resulting cleavage energy is plotted in Figure 4a. It can be seen that the total energy increases with the separation *d* and gradually converges to the ideal cleavage cohesion energy of about 0.20 J m^{-2}. The latter is
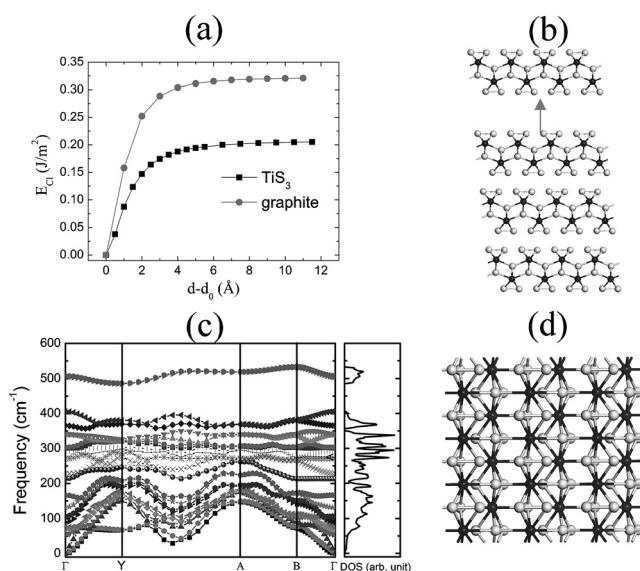
Figure 4. a) Cleavage energy E_{cl} as a function of the separation between two TiS$_3$ monolayers, the E_{cl} for graphite is also plotted for comparison. b) Schematic view of the exfoliation of a TiS$_3$ monolayer from bulk, c) phonon band structure and density of states of TiS$_3$ monolayer, and d) snapshot of TiS$_3$ monolayer at 8 ps of the BOMD simulation in the NPT ensemble at 300 K and 0 GPa.

notably less than the cleavage cohesion energy of graphite, which is about $0.32\ \mathrm{J\,m^{-2}}$ from our calculation or $0.36\ \mathrm{J\,m^{-2}}$ from experiment.[26] The smaller cleavage cohesion energy of TiS_3, compared to that of graphite, suggests that the exfoliation of bulk TiS_3 should be highly feasible experimentally. Indeed, monolayer TiS_3 has been recently isolated (see the Note added during review), and the measured optical gap is about 1 eV, nearly the same as the computed HSE06 bandgap (1.06 eV). The stability of the TiS_3 monolayer is another issue that should be examined. First, we compute the phonon spectrum of the TiS_3 monolayer, based on density functional perturbation theory with the linear response as implemented in the QUANTUM-ESPRESSO package.[27] As shown in Figure 4c, the TiS_3 show no imaginary phonon mode, indicating its dynamical stability. Next, we perform BOMD simulations. The constant-temperature (300 K) and -pressure (0 GPa) (NPT) is adopted. Here, the time step is 2 fs, and the total simulation time is 8 ps. As shown in Figure 4d, the in-plane structure integrity of the TiS_3 monolayer is well kept during the BOMD run, suggesting good thermal stability of the TiS_3 monolayer.

In summary, we predict a new 2D material, TiS_3 monolayer sheet, which is a semiconductor with a desired direct bandgap of about 1 eV. The electron mobilities of the TiS_3 monolayer are dominant and highly anisotropic. More specifically, the electron mobility along the b direction exhibits a very high value of $13.87 \times 10^3\ \mathrm{cm^2\,V^{-1}\,s^{-1}}$, rendering the TiS_3 monolayer particularly attractive for future applications in nanoelectronics as its mobility is even notably higher than that of the MoS_2 monolayer. The computed ideal cleavage cohesion energy for TiS_3 is about $0.20\ \mathrm{J\,m^{-2}}$, less than that of graphite, indicating the isolation of a 2D TiS_3 monolayer can be technically attainable by either liquid exfoliation or mechanical cleavage as done for the isolation of 2D graphene or MoS_2 sheet.[15,16] Lastly, dynamic and thermal stability of TiS_3 is confirmed by both phonon spectrum and BOMD simulations. Thus, we expect that fabrication of 2D TiS_3 monolayer and measurement of its electronic properties will be likely accomplished in the near future.

Experimental Section

For the 2D TiS_3 monolayer sheet, geometrical optimization and electronic structure calculations are carried out using density functional theory (DFT) methods within the generalized gradient approximation (GGA) and with the Perdew–Burke–Ernzerhof (PBE) exchange correlation functional, as implemented in the Vienna ab initio simulation package (VASP).[28] The Grimme's D2 dispersion correction[29] is adopted to account for the long-range vdW interactions. The ion–electron interaction is treated using the projector-augment-wave (PAW) technique and a kinetic energy cut of 500 eV is chosen. A vacuum space of $\approx 20\ \text{Å}$ along the direction normal to the monolayer plane is undertaken so that the interlayer interaction due to the periodic boundary condition can be neglected. For the geometric optimization, a $7 \times 10 \times 1$ Monkhorst-Pack[30] grid is used and all structures are relaxed until the forces on the atoms are less than $0.01\ \mathrm{eV\,\text{Å}^{-1}}$, and the total energy change becomes less than 1.0×10^{-5} eV. For total energy calculations, a fine $35 \times 50 \times 1$ grid is adopted. Since the PBE functional tends to underestimate the bandgap of semiconductors, the hybrid HSE06 functional[31] is also used to compute the bandgap of optimized TiS_3 monolayer sheet.

The carrier mobility (μ) is calculated based on the deformation theory proposed by Bardeen and Shockley.[32] Due to the fact that for inorganic semiconductors, the coherent wavelength of thermally activated electrons or holes is close to the acoustic phonon wavelength and is much longer than typical bond length, the scattering of a thermal electron or hole is dominated by the electron-acoustic phonon coupling.[32] The deformation theory has been widely used to evaluate μ of low-dimensional systems.[11a,21–24,33] On the basis of effective mass approximation, the charge mobility in 2D materials can be expressed as:

$$\mu = \frac{2e\hbar^3 C}{3k_B T |m^*|^2 E_1^2} \tag{1}$$

Here, C is the elastic modulus defined as $C = [\partial E/\partial \delta^2]/S^0$, in which E is the total energy of the system (per supercell), and δ is the applied uniaxial strain, and S^0 is the area of the optimized 2D structure. m^* is the effective mass, which can be given as $m^* = \hbar^2 (\partial E/\partial k^2)^{-1}$ (in which $\hbar$ is the Planck's constant and k is the magnitude of the wave-vector in momentum space), T is the temperature, and E_1 is the deformation potential constant, which is proportional to the band edge shift induced by the strain. E_1 is defined as $\Delta E = E_1(\Delta l/l_0)$, in which ΔE is the energy shift of the band edge position with respect to the lattice dilation $\Delta l/l_0$ along the direction a or b, the energies of the band edges are calculated with respect to the vacuum level.

Note added during Review. During the review, we received a manuscript from the group of Castellanos-Gomez who informed us that their group has successfully isolated TiS_3 monolayer sheets.[34]

[1] K. S. Novoselov, A. K. Geim, S. Morozov, D. Jiang, Y. Zhang, S. Dubonos, I. Grigorieva, A. Firsov, *Science* **2004**, *306*, 666–669.

[2] a) S. Z. Butler, S. M. Hollen, L. Cao, Y. Cui, J. A. Gupta, H. R. Gutierrez, T. F. Heinz, S. S. Hong, J. Huang, A. F. Ismach, *ACS Nano* **2013**, *7*, 2898–2926; b) K. J. Koshi, Y. Cui, *ACS Nano* **2013**, *7*, 3739–3743.

[3] a) Y. Zhang, Y.-W. Tan, H. L. Stormer, P. Kim, *Nature* **2005**, *438*, 201–204; b) K. Novoselov, A. K. Geim, S. Morozov, D. Jiang, M. K. I. Grigorieva, S. Dubonos, A. Firsov, *Nature* **2005**, *438*, 197–200; c) A. K. Geim, K. S. Novoselov, *Nat. Mater.* **2007**, *6*, 183–191; d) A. Castro Neto, F. Guinea, N. Peres, K. S. Novoselov, A. K. Geim, *Rev. Mod. Phys.* **2009**, *81*, 109.

[4] a) Q. H. Wang, K. Kalantar-Zadeh, A. Kis, J. N. Coleman, M. S. Strano, *Nat. Nanotechnol.* **2012**, *7*, 699–712; b) M. Chhowalla, H. S. Shin, G. Eda, L.-J. Li, K. P. Loh, H. Zhang, *Nat. Chem.* **2013**, *5*, 263–275.

[5] a) H. Zeng, C. Zhi, Z. Zhang, X. Wei, X. Wang, W. Guo, Y. Bando, D. Golberg, *Nano Lett.* **2010**, *10*, 5049–5055; b) L. Song, L. Ci, H. Lu, P. B. Sorokin, C. Jin, J. Ni, A. G. Kvashnin, D. G. Kvashnin, J. Lou, B. I. Yakobson, *Nano Lett.* **2010**, *10*, 3209–3215.

[6] a) L. Chen, C.-C. Liu, B. Feng, X. He, P. Cheng, Z. Ding, S. Meng, Y. Yao, K. Wu, *Phys. Rev. Lett.* **2012**, *109*, 056804; b) B. Feng, Z. Ding, S. Meng, Y. Yao, X. He, P. Cheng, L. Chen, K. Wu, *Nano Lett.* **2012**, *12*, 3507–3511; c) P. Vogt, P. De Padova, C. Quaresima, J. Avila, E. Frantzeskakis, M. C. Asensio, A. Resta, B. Ealet, G. Le Lay, *Phys. Rev. Lett.* **2012**, *108*, 155501.

[7] M. Dávila, L. Xian, S. Cahangirov, A. Rubio, G. Le Lay, *New J. Phys.* **2014**, *16*, 095002.

[8] a) L. Li, Y. Yu, G. J. Ye, Q. Ge, X. Ou, H. Wu, D. Feng, X. H. Chen, Y. Zhang, *Nat. Nanotechnol.* **2014**, *9*, 372–377; b) H. Liu,

A. T. Neal, Z. Zhu, Z. Luo, X. Xu, D. Tománek, P. D. Ye, *ACS Nano* **2014**, *8*, 4033 – 4041.

[9] B. Partoens, F. Peeters, *Phys. Rev. B* **2006**, *74*, 075404.

[10] K. F. Mak, C. Lee, J. Hone, J. Shan, T. F. Heinz, *Phys. Rev. Lett.* **2010**, *105*, 136805.

[11] a) J. Qiao, X. Kong, Z.-X. Hu, F. Yang, W. Ji, *Nat. Commun.* **2014**, *5*, 4475; b) V. Tran, R. Soklaski, Y. Liang, L. Yang, *Phys. Rev. B* **2014**, *89*, 35319; c) J. Dai, X. C. Zeng, *J. Phys. Chem. Lett.* **2014**, *5*, 1289 – 1293; d) H. Guo, N. Lu, J. Dai, X. Wu, X. C. Zeng, *J. Phys. Chem. C* **2014**, *118*, 14051 – 14059.

[12] a) Y. Wu, Y.-m. Lin, A. A. Bol, K. A. Jenkins, F. Xia, D. B. Farmer, Y. Zhu, P. Avouris, *Nature* **2011**, *472*, 74 – 78; b) F. Schwierz, *Nat. Nanotechnol.* **2010**, *5*, 487 – 496; c) L. Liao, Y.-C. Lin, M. Bao, R. Cheng, J. Bai, Y. Liu, Y. Qu, K. L. Wang, Y. Huang, X. Duan, *Nature* **2010**, *467*, 305 – 308.

[13] a) Y. Yoon, K. Ganapathi, S. Salahuddin, *Nano Lett.* **2011**, *11*, 3768 – 3773; b) B. Radisavljevic, A. Radenovic, J. Brivio, V. Giacometti, A. Kis, *Nat. Nanotechnol.* **2011**, *6*, 147 – 150.

[14] a) L. Brattås, A. Kjekshus, *Acta Chem. Scand.* **1972**, *26*, 3441 – 3449; b) S. Furuseth, L. Brattas, A. Kjekshus, *Acta Chem. Scand.* **1975**, *29*, 623.

[15] a) V. Nicolosi, M. Chhowalla, M. G. Kanatzidis, M. S. Strano, J. N. Coleman, *Science* **2013**, *340*, 6139; b) J. N. Coleman, M. Lotya, A. O'Neill, S. D. Bergin, P. J. King, U. Khan, K. Young, A. Gaucher, S. De, R. J. Smith, *Science* **2011**, *331*, 568 – 571.

[16] K. Novoselov, D. Jiang, F. Schedin, T. Booth, V. Khotkevich, S. Morozov, A. Geim, *Proc. Natl. Acad. Sci. USA* **2005**, *102*, 10451 – 10453.

[17] a) E. Finkman, B. Fisher, *Solid State Commun.* **1984**, *50*, 25 – 28; b) P.-L. Hsieh, C. Jackson, G. Grüner, *Solid State Commun.* **1983**, *46*, 505 – 507.

[18] H. G. Grimmeiss, A. Rabenau, H. Hahn, P. Ness, *Z. Elektrochem.* **1961**, *65*, 776 – 783.

[19] a) I. Ferrer, J. Ares, J. Clamagirand, M. Barawi, C. Sánchez, *Thin Solid Films* **2013**, *535*, 398 – 401; b) I. Ferrer, M. Maciá, V. Carcelén, J. Ares, C. Sánchez, *Energy Procedia* **2012**, *22*, 48 – 52.

[20] J. O. Island, M. Buscema, M. Barawi, J. M. Clamagirand, J. R. Ares, C. Sánchez, I. J. Ferrer, G. A. Steele, H. S. van der Zant, A. Castellanos-Gomez, *Adv. Opt. Mater.* **2014**, *2*, 641 – 645.

[21] Y. Cai, G. Zhang, Y.-W. Zhang, *J. Am. Chem. Soc.* **2014**, *136*, 6269.

[22] J. Chen, J. Xi, D. Wang, Z. Shuai, *J. Phys. Chem. Lett.* **2013**, *4*, 1443.

[23] J. Xi, M. Long, L. Tang, D. Wang, Z. Shuai, *Nanoscale* **2012**, *4*, 4348.

[24] M. Long, L. Tang, D. Wang, Y. Li, Z. Shuai, *ACS Nano* **2011**, *5*, 2593.

[25] a) X. Li, X. Wu, J. Yang, *J. Am. Chem. Soc.* **2014**, *136*, 11065; b) B. Sachs, T. Wehling, K. Novoselov, A. Lichtenstein, M. Katsnelson, *Phys. Rev. B* **2013**, *88*, 201402.

[26] R. Zacharia, H. Ulbricht, T. Hertel, Phys. Rev. B **2004**, *69*, 155406.

[27] P. Giannozzi, S. Baroni, N. Bonini, M. Calandra, R. Car, C. Cavazzoni, D. Ceresoli, G. L. Chiarotti, M. Cococcioni, I. Dabo *et al.*, J. Phys. Codens. Matter. **2009**, 21, 395502.

[28] G. Kresse, J. Furthmüller, *Phys. Rev. B* **1996**, *54*, 11169.

[29] S. Grimme, J. Antony, S. Ehrlich, H. Krieg, *J. Chem. Phys.* **2010**, *132*, 154104.

[30] H. J. Monkhorst, J. D. Pack, *Phys. Rev. B* **1976**, *13*, 5188.

[31] J. Heyd, G. E. Scuseria, M. Ernzerhof, *J. Chem. Phys.* **2006**, *124*, 219906.

[32] J. Bardeen, W. Shockley, *Phys. Rev.* **1950**, *80*, 72.

[33] M.-Q. Long, L. Tang, D. Wang, L. Wang, Z. Shuai, *J. Am. Chem. Soc.* **2009**, *131*, 17728.

[34] J. O. Island, M. Barawi, R. Biele, A. Almazán, J. M. Clamagirand, J. R. Ares, C. Sánchez, H. S. van der Zant, J. V. Álvarez, R. D'Agosta, I. J. Ferrer, A. Castellanos-Gomez, *Adv. Mater.* **2015**, 27, 2595 .